



# Mie Resonator Color Inks of Monodispersed and Perfectly Spherical Crystalline Silicon Nanoparticles

Sugimoto, Hiroshi  
Okazaki, Takuma  
Fujii, Minoru

---

**(Citation)**

Advanced Optical Materials, 8(12):2000033-2000033

**(Issue Date)**

2020-06-18

**(Resource Type)**

journal article

**(Version)**

Version of Record

**(Rights)**

© 2020 The Authors. Published by WILEY - VCH Verlag GmbH & Co. KGaA, Weinheim.  
This is an open access article under the terms of the Creative Commons Attribution License, which permits use, distribution and reproduction in any medium, provided the original work is properly cited.

**(URL)**

<https://hdl.handle.net/20.500.14094/90007161>



# Mie Resonator Color Inks of Monodispersed and Perfectly Spherical Crystalline Silicon Nanoparticles

Hiroshi Sugimoto,\* Takuma Okazaki, and Minoru Fujii

A crystalline silicon (Si) nanoparticle (NP) of 100–200 nm in diameter exhibits a highly saturated color owing to Mie resonance, and can be a component to realize angle-insensitive structural color covering the entire visible range. However, to date, coloring a substrate by Si nanostructures has only been achieved in a very small area by using electron beam lithography and dry etching processes. In this work, a Si NP color ink capable of coloring a flexible substrate by a painting process is developed. The sphericity of Si NPs is very high; the circularity factor obtained from a transmission electron microscope image reaches 0.97. The average diameter of Si nanospheres is controlled from 95 to 200 nm, and the polydispersity defined by the standard deviation divided by the average diameter is as small as 6%. Because of the high sphericity, high crystallinity, high size purity, and perfect dispersion in solution, the Si nanosphere solutions exhibit vivid colors recognizable by naked eye in a range of blue to orange. The Si nanosphere color inks combined with a polymer binder are capable of coloring flexible substrates by a painting process.

noble metal nanostructures is nonfading and noniridescent.<sup>[5,6]</sup> Because plasmonic coloration uses resonant light scattering and/or absorption of individual nano-objects as color pixels, high-resolution color printing ( $\approx 100\,000$  dpi) exceeding the optical diffraction limit can be achieved.<sup>[6–9]</sup> However, a fundamental limitation of plasmonic coloration is that complex shapes (structures) such as multilayered and asymmetric metal-dielectric nanostructures are necessary to achieve high color purity in a wide color range.<sup>[6–10]</sup> The complex shape (structure) often results in polarization-sensitive and iridescent coloration.

Recently, nanostructures of high-refractive-index dielectrics having electric dipole (ED) and magnetic dipole (MD) Mie resonances in the visible range have emerged as an alternative to plasmonic

## 1. Introduction


Typical pigments composed of organic dyes absorb a certain region of the visible light spectrum, and the complementary color is recognizable by the human eye. Because excited organic dyes are not chemically stable, their colors fade over time under exposure to light. Structural color generated by optical interactions of light with nano- and microstructures have attracted considerable research and industrial attention because the color never diminishes as long as the structure is preserved.<sup>[1–4]</sup> Historically, structural coloration has utilized the interference of light in a periodic structure of subwavelength components, and thus the color depended on the viewing angle. In contrast, structural color based on surface plasmon resonances of

nanostructures.<sup>[11–16]</sup> Among high-refractive-index dielectric materials,<sup>[17]</sup> crystalline silicon (Si) nanostructures have been most widely studied as a component to realize structural coloration. A spherical Si nanocrystal with a diameter in the 100–200 nm range has ED and MD Mie resonances in the visible range.<sup>[11,18,19]</sup> Color pixels with highly saturated scattering colors have been produced by nanodisks<sup>[15]</sup> and nanoblocks<sup>[14]</sup> as well as nanospheres of Si crystal, and high-resolution color printing has been achieved by using these color pixels. However, the printing is limited to a very small area (typically smaller than  $1\text{ mm}^2$ )<sup>[20–22]</sup> owing to the restriction of the fabrication processes involving electron beam lithography.

As a method to realize large-area structural coloration by nanoparticles (NPs), coating or inkjet printing of NP ink is proposed.<sup>[23,24]</sup> Several methods have been proposed for the fabrication of a Si NP solution. One widely used method is the laser ablation of a Si wafer in inert gas<sup>[11,18]</sup> or in a solution.<sup>[25]</sup> However, the size and shape distributions of nanoparticles produced by these methods are very large, and the solution cannot be used as an ink for structural coloration. Another method to produce spherical Si particles is chemical vapor deposition with disilane or trisilane as precursor gas.<sup>[26,27]</sup> However, the spheres produced by this method are made of amorphous Si, which has a much larger imaginary part in the dielectric permittivity than the crystalline Si and is not suitable for structural coloration. Recently, fabrication of a large amount of crystalline Si NPs by a simple grinding process was reported.<sup>[28]</sup> However, the process cannot control the NP shape, and the average circularity factor of the particles is  $\approx 0.8$ , which is far from a spherical shape. Because of the shape and size distributions, the colloidal dispersions are

Dr. H. Sugimoto, T. Okazaki, Prof. M. Fujii  
Department of Electrical and Electronic Engineering  
Graduate School of Engineering  
Kobe University  
Rokkodai, Nada Ward, Kobe 657-8501, Japan  
E-mail: sugimoto@eedept.kobe-u.ac.jp

Dr. H. Sugimoto  
JST-PRESTO  
Honcho 4-1-8, Kawaguchi, Saitama 332-0012, Japan

 The ORCID identification number(s) for the author(s) of this article can be found under <https://doi.org/10.1002/adom.202000033>.

© 2020 The Authors. Published by WILEY-VCH Verlag GmbH & Co. KGaA, Weinheim. This is an open access article under the terms of the Creative Commons Attribution License, which permits use, distribution and reproduction in any medium, provided the original work is properly cited.

DOI: 10.1002/adom.202000033

brownish and cannot be used as color inks. To realize structural color inks composed of Si Mie resonators, high size purity, high shape uniformity, and high crystallinity must be achieved.

Recently, we developed a process to produce a solution in which spherical NPs of Si crystal are dispersed. The method includes the sputter-deposition of silicon suboxide ( $\text{SiO}_x$ ), disproportionation of  $\text{SiO}_x$  into Si NPs and a  $\text{SiO}_2$  matrix, and extraction of Si NPs from the matrix.<sup>[29]</sup> Because of the almost perfectly spherical shape of Si NPs produced by this process, the scattering spectra of individual NPs agree very well with the calculated spectra.<sup>[30]</sup> However, owing to the size distribution, the color of the solution was brownish and similar to the case in Ref. [28]. Another drawback of the process is that it is not scalable because the process involves a slow sputter-deposition process.

The purpose of this work is to develop a high-quality color ink composed of crystalline Si NPs for the structural coloration of an arbitrary substrate. To achieve this purpose, three important processes are introduced. The first one involves using commercially available silicon monoxide (SiO) powder instead of sputter-deposited  $\text{SiO}_x$  as a starting material. This makes it possible to scale up the production of Si NPs from the mg to the g range. The second process involves the optimization of the temperature for the solid-state disproportionation of SiO into Si and  $\text{SiO}_2$ . We show that the temperature should be higher than the melting point of bulk Si crystal (1414 °C) but lower than that of silica (1710 °C). In the temperature range, perfectly spherical liquid droplets of Si are formed in a silica matrix, and the shape is frozen during the cooling process, resulting in perfectly spherical crystalline Si particles [Si nanospheres (Si NSs)]. The sphericity and shape uniformity are much better than those of Si NPs grown by a lower-temperature process. The third important process is the precise size separation of Si NSs by the density gradient centrifugation process. By dramatically reducing the size distribution, we succeeded in coloring solutions of Si NSs in the blue-to-orange range. We demonstrate the structural coloration of a flexible substrate (>1 cm<sup>2</sup> in area) by Si NS color inks.

## 2. Results and Discussion

### 2.1. Preparation of the Colloidal Dispersion

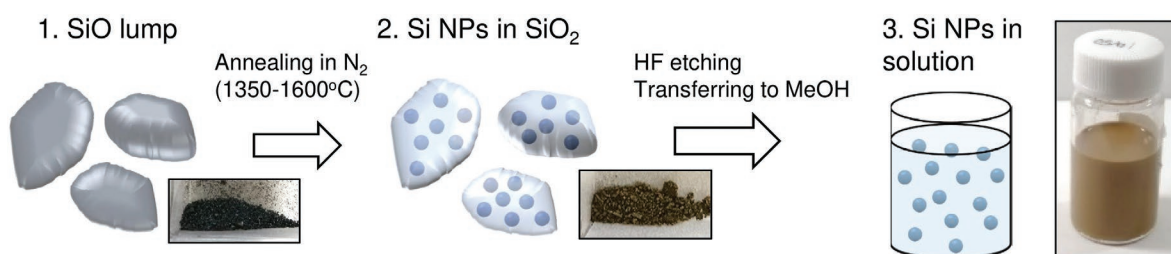
In this work, we first prepare a colloidal dispersion of Si NSs and then produce color inks by a size separation process. **Scheme 1** shows the procedure for the production of the colloidal dispersion. SiO lumps (several mm in size) were crushed to powder and annealed at 1350–1600 °C in an inert

gas atmosphere for 10–30 min to promote the solid-state disproportionation of SiO into Si and  $\text{SiO}_2$ . Etching out  $\text{SiO}_2$  matrices in a hydrofluoric acid (HF) solution results in the extraction of freestanding Si NPs. The extracted NPs are transferred to methanol, followed by a minute ultrasonication. The etching process takes less than 1 h.

### 2.2. Size, Sphericity and Crystallinity of the Si Nanoparticles

**Figure 1a–d** shows transmission electron microscope (TEM) (JEM-2100F; JEOL) images of Si NPs grown at 1400, 1425, 1450, and 1500 °C for 30 min. The scale bars are different between **Figure 1a–d**. A scanning electron microscope (SEM) image of Si NPs grown at 1500 °C is shown in **Figure 1e**. In **Figure 1f**, average diameters obtained from TEM and SEM images are plotted as a function of the growth temperature. The error bars are the standard deviations obtained from the size distribution analyses (**Figure S1** in the Supporting Information). From the TEM and SEM images and the growth temperature dependence of the size, we notice a discontinuous change between 1400 and 1425 °C: the average diameter dramatically increases, and the NP shape changes from nonspherical to spherical. These discontinuous changes suggest that the NP growth mode is changed below and above the bulk Si melting point (1414 °C). Below this temperature, NPs are grown by a solid-state Ostwald-ripening growth process. In contrast, above the bulk Si melting point, spherical droplets of melted Si particles are formed in softened  $\text{SiO}_2$  matrices, and the droplets grow by absorbing dissolved small particles. In fact, the magnified image of a Si NS grown at 1425 °C in the inset of **Figure 1b** shows the attachment of extremely small particles (<5 nm) about to be absorbed by a large Si NS. During the cooling process, the shape of the spherical droplets is preserved, resulting in the formation of almost perfectly spherical NPs.

The discontinuity at the bulk melting point also appears in the solution dispersibility. Above the bulk Si melting point, the size measured by dynamic light scattering (DLS) [**Figure 1f** (red open squares)] agrees very well with that obtained by electron microscope (EM) observations. This means that Si NSs are perfectly dispersed in a solution without agglomeration. In fact, we can see perfectly isolated Si NSs in an SEM image of a substrate on which a diluted Si NSs solution is dropped (**Figure S2** in the Supporting Information). The zeta potential (Zetasizer Nano, Malvern) of Si NSs (1450 °C) in water is  $-12.8 \pm 2.1$  mV. The negative potential is probably owing to the Si-OH bonds formed on the surface of Si NSs, and might be partly responsible for the water solubility. However, the potential is not large



**Scheme 1.** Preparation procedure for colloidal dispersion of Si NPs.

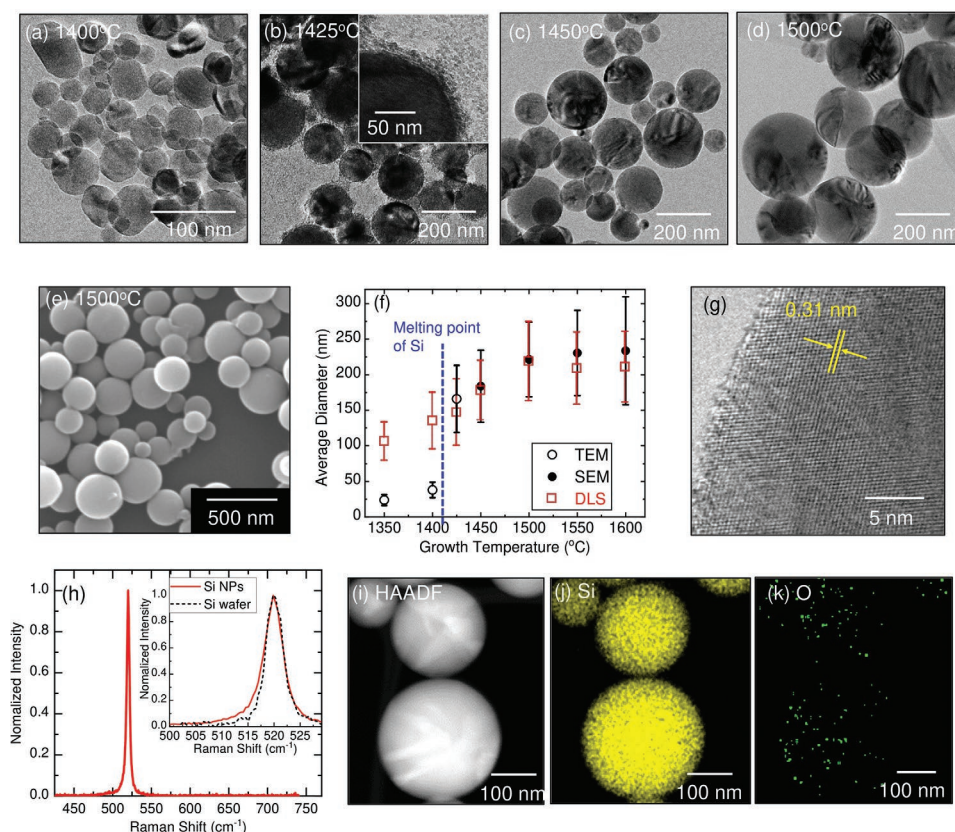


**Figure 1.** a–d) TEM images of Si NPs grown at different temperatures. e) SEM image of Si NSs grown at 1500 °C. f) Average diameters obtained from electron microscope [TEM (black open circles) and SEM (black filled circles)] and DLS (red open squares) as a function of growth temperature. g) High-resolution TEM image of Si NS (1500 °C). h) Raman scattering spectrum of Si NSs (1500 °C). Inset: Comparison with spectrum of Si wafer. i) HAADF-STEM and j,k) EDS mapping images (yellow: Si, green: O) of Si NSs.

enough to explain the dispersibility solely by electrostatic repulsions, and the mechanism of the high solution dispersibility is still under debate. In the case of Si NPs grown at temperatures below the bulk Si melting point, the DLS diameters are much larger than the EM diameters, indicating the aggregation of Si NPs in solution. As high solution dispersibility and high sphericity are essential for the production of high-quality Si NS inks,<sup>[18]</sup> from now on, we focus on Si NSs grown at temperatures higher than the bulk melting point.

We first analyze the sphericity of Si NSs quantitatively using two different factors that provide complementary information. The circularity factor ( $c$ ) defined as  $c = 4\pi A/p$ , where  $A$  is the area and  $p$  is the perimeter of a particle in the 2D projection, respectively, of NSs grown at 1450 °C is 0.97 on average (see Figure S3 in the Supporting Information). This value is much higher than the previously reported value for Si NPs (0.81).<sup>[28]</sup> In addition, the roundness factor ( $r$ ) defined as  $r = 4A/\pi d_F^2$ , where  $d_F$  is the maximum Feret's diameter, is 0.98 on average. This value is almost the same as that reported for spherical Au NPs of around 100 nm in diameter (0.96).<sup>[31]</sup>

Another important factor affecting the quality of the Mie resonance is the crystallinity of NSs. Figure 1g shows a high-resolution TEM image of a Si NS grown at 1500 °C. Lattice fringes corresponding to {111} planes of Si crystal can be seen clearly. Figure 1h shows a Raman scattering spectrum of Si NSs grown at 1500 °C together with that of bulk Si crystal. The sharp peak

of the transverse optical (TO) phonon mode at 520 cm<sup>-1</sup> indicates high crystallinity, although it is slightly broadened owing to the existence of the surface.<sup>[32]</sup> Figure 1i–k shows a high-angle annular dark-field (HAADF) scanning TEM image and energy-dispersive X-ray spectroscopy (EDS) mapping of elemental Si and oxygen (O) of the same Si NSs. The images confirm that no thick oxides are formed on the surface of the NSs.

### 2.3. Mie Scattering

Prior to developing Si NS inks from colloidal dispersion, we study the Mie scattering property of individual Si NSs. Figure 2a shows the backward scattering spectra and corresponding scattering images of different sizes of single Si NSs grown at 1450 °C and placed on a glass substrate. The scattering color changes depending on the diameter of the Si NSs. In Figure 2a, calculated backward scattering spectra are also shown (dashed gray lines). For the calculation, the glass substrate is not taken into account, i.e., Si NS is placed in air, but the experimental incident angle and detection cone are taken into account. Due to the high sphericity and crystallinity of Si NSs, the measured and calculated spectra are in good agreement. This slight discrepancy is mainly owing to the presence of a silica substrate; the ED mode is broadened owing to the interaction with the substrate.<sup>[11]</sup> To evaluate the scattering color of the Si NSs, the

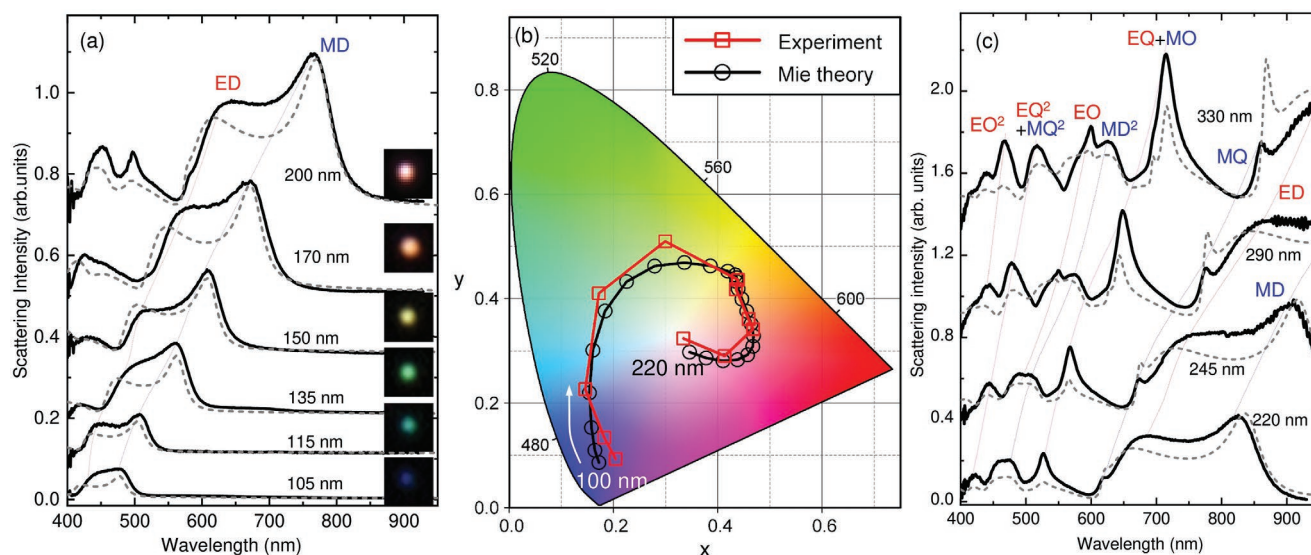


**Figure 2.** a) Scattering spectra of single Si NSs (grown at 1450 °C) with different diameters (105–200 nm in diameter) placed on glass substrate. Corresponding dark field images are shown. b) CIE1931 chromaticity diagram and experimental color space values obtained from scattering spectra of single Si NSs of different diameters (100–220 nm). Data obtained from calculated scattering spectra are also shown. c) Scattering spectra of Si NSs (grown at 1500 °C) of different diameters (220–330 nm in diameter) placed on glass substrate.

scattering spectra are converted into the CIE1931 color space. Figure 2b shows data obtained from the measured and calculated spectra of Si NSs in a size range of 100–220 nm. The results cover a wide range of the visible range.

In Figure 2c, the scattering spectra of larger Si NSs (>220 nm in diameter) grown at 1500 °C having ED and MD modes in the near-infrared range are shown. Electric and magnetic multipoles such as the quadrupole (EQ and MQ) and octupole (EO and MO) modes are clearly observed; the assignment of resonant modes is shown in the Supporting Information (Figure S4, Supporting Information). In addition, higher-order modes in the radial direction ( $ED^2$ ,  $MD^2$ ,  $EQ^2$ ,  $MQ^2$ , and  $EO^2$ ) are observed.<sup>[33]</sup> The good agreement between the measured and calculated spectra can also be seen in the range of the higher-order modes.

## 2.4. Preparation of the Color Ink

After confirming that individual Si NSs show almost ideal Mie scattering spectra, we proceed to the production of high-quality color inks. Figure 3a shows the extinction spectra of the colloidal dispersion of Si NSs with different growth temperatures ( $T_G$ ) and times. The extinction spectra are obtained from the transmittance spectra of solutions in 10-mm optical path cubicles. Although the size-dependent shift of the Mie resonance is observed, the resonance is very broad, and the color of the solutions is always brownish (see Scheme 1). The polydispersity, defined as the standard deviation ( $\sigma$ ) divided by the average diameter ( $D_{ave}$ ) of the pristine colloidal dispersion, is in the range of 30–35%.

To separate a pristine colloidal dispersion into solutions of size-purified Si NSs, we employ a sucrose density gradient centrifugation process.<sup>[34]</sup> Figure 3b displays the Si NS (grown at 1450 °C for 10 min) solutions before and after the centrifugation process (see Experimental section for details). The

brownish color of the pristine solution is separated into colored layers. The color changes from blue to orange from the top to the bottom. By collecting small amounts of solutions from the top, we obtain solutions of different colors. Figure 3c shows the separated solutions under white light emitting diode (LED) illumination. Colored solutions of Si NSs are successfully produced. It is worth noting that the solutions of size-separated Si NSs exhibit bright green, yellow, and orange colors even under room light (Figure S5 in the Supporting Information).

Figure 3d,e shows a representative TEM image of size-separated Si NSs and the size distribution obtained from the TEM images, respectively. Additional TEM images are shown in the Supporting Information (Figure S6, Supporting Information). The average diameter and the standard deviation are 162 and 10.6 nm, respectively. The polydispersity ( $\sigma/D_{ave}$ ) decreased to 6.5%.

The dramatic reduction of the polydispersity significantly affects the optical properties of the solutions. Figure 3f shows an extinction spectrum of a size-separated solution. The spectrum is significantly narrower than those of the pristine solutions in Figure 3a, and is only slightly broader than the calculated scattering spectrum of a single Si NS (dashed blue curve in Figure 3f,  $D = 159$  nm) exhibiting the MD peak at the same wavelength. We tried to reproduce the measured extinction spectrum from the calculated spectra of single Si NSs by assuming a normal size distribution with  $D_{ave}$  and  $\sigma$  as fitting parameters. The calculated spectrum is shown by a dashed red curve in Figure 3f. The best fit is obtained when  $D_{ave}$  and  $\sigma$  are 159 and 9.5 nm, respectively. This corresponds to a polydispersity of 6.0%, which is very close to the value obtained from TEM observations. Good reproduction of the measured extinction spectrum just by taking into account the size distribution guarantees high shape uniformity and the perfect dispersion of Si NSs in the solution.

To evaluate the scattering color of size-separated Si NS solutions, we measured the diffuse reflection spectra using the setup

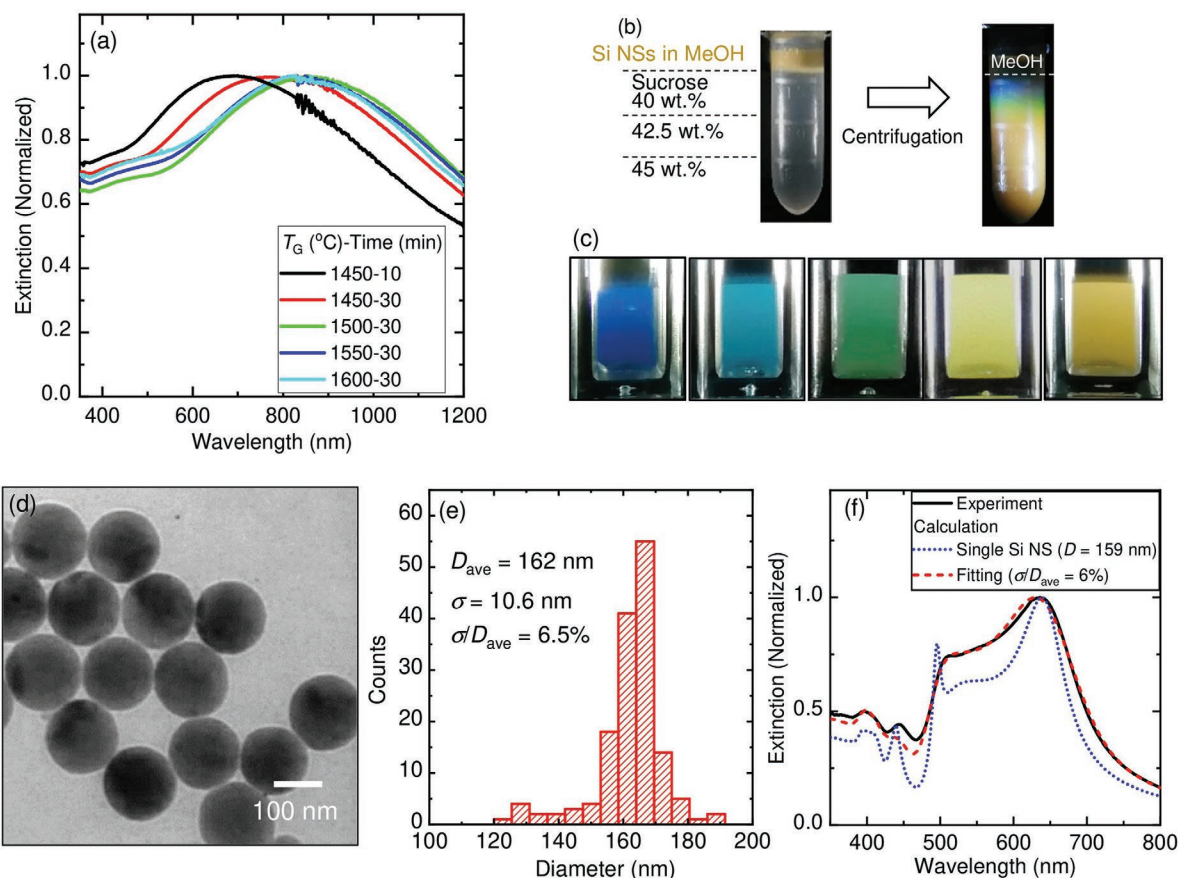


**Figure 3.** a) Normalized extinction spectra of Si NSs grown at different temperatures and times. b) Photographs of tube before and after centrifugation in density gradient centrifugation size separation process. c) Photographs of solutions of size-separated Si NSs. d) Typical TEM image and e) size distribution of Si NSs in size-separated solution. f) Measured extinction spectrum of size-separated Si NS solution (solid black line) and calculated spectrum of single Si NS (dotted blue curve). Spectrum of ensemble of Si NSs obtained by fitting measured spectrum by assuming normal distribution is also shown (dashed red curve).  $D_{ave}$  and  $\sigma$  obtained by fitting are 159 and 9.5 nm, respectively.

shown in **Figure 4a**. In this setup, light scattered to the backward direction except for the specular reflection is collected by an integrating sphere. **Figure 4b** shows the normalized diffuse reflection spectra of Si NSs with diameters ranging from 95 to 200 nm. The corresponding extinction spectra are shown in the Supporting Information (**Figure S7**, Supporting Information). We can see sharp reflection peaks. The peak shifts from 420 to 700 nm when increasing the Si NS size. The measured diffuse reflection spectra are converted into the CIE1931 color space and are plotted in **Figure 4c** (filled black circles) together with the data converted from the calculated backward scattering spectra of single Si NSs in methanol ( $n = 1.33$ ) (95–200 nm in diameter). The solutions exhibit size-dependent colors in a wide range, although the color gamut is slightly smaller than that of single Si NSs.

## 2.5. The Painting Process

Finally, we develop a process to color a substrate by Si NS inks. To color a substrate to the same color as the solution, it is necessary to solidify the ink by maintaining a NS-to-NS distance that is larger than  $\approx 50$  nm.<sup>[14,15,35]</sup> To achieve this, we first mixed a methanol solution of Si NSs with polyvinylpyrrolidone

(PVP) solution, and then drop-cast the mixture solution on a substrate. PVP acts as an optically transparent binder and prevents the agglomeration of Si NSs after evaporation of the solvent. The insets of **Figure 4d–g** show photographs of the Si NS inks and Si NSs-PVP films on glass substrates illuminated by a white LED. We can see that the substrates exhibit structural colors very similar to those of the inks. The diffuse reflectance spectra of the inks and substrates are shown in **Figure 4d–g**. The spectra are very similar, although those of the substrates are slightly red-shifted compared to those of the solutions. The long wavelength shift is probably owing to changes in the refractive indices of the matrices from methanol (1.33) to PVP ( $\approx 1.5$ ). Since the procedure does not require any heating processes, it can be applied to flexible substrates. **Figure 4h** shows a photo of a Si NSs-PVP film on a PET film (0.125 mm in thickness). As shown in **Figure 4i**, the color is sustained even when it is bent at a bending radius of 9 mm.

## 3. Conclusion

In summary, we developed structural color inks of Si NSs. Three newly devised processes are responsible for the

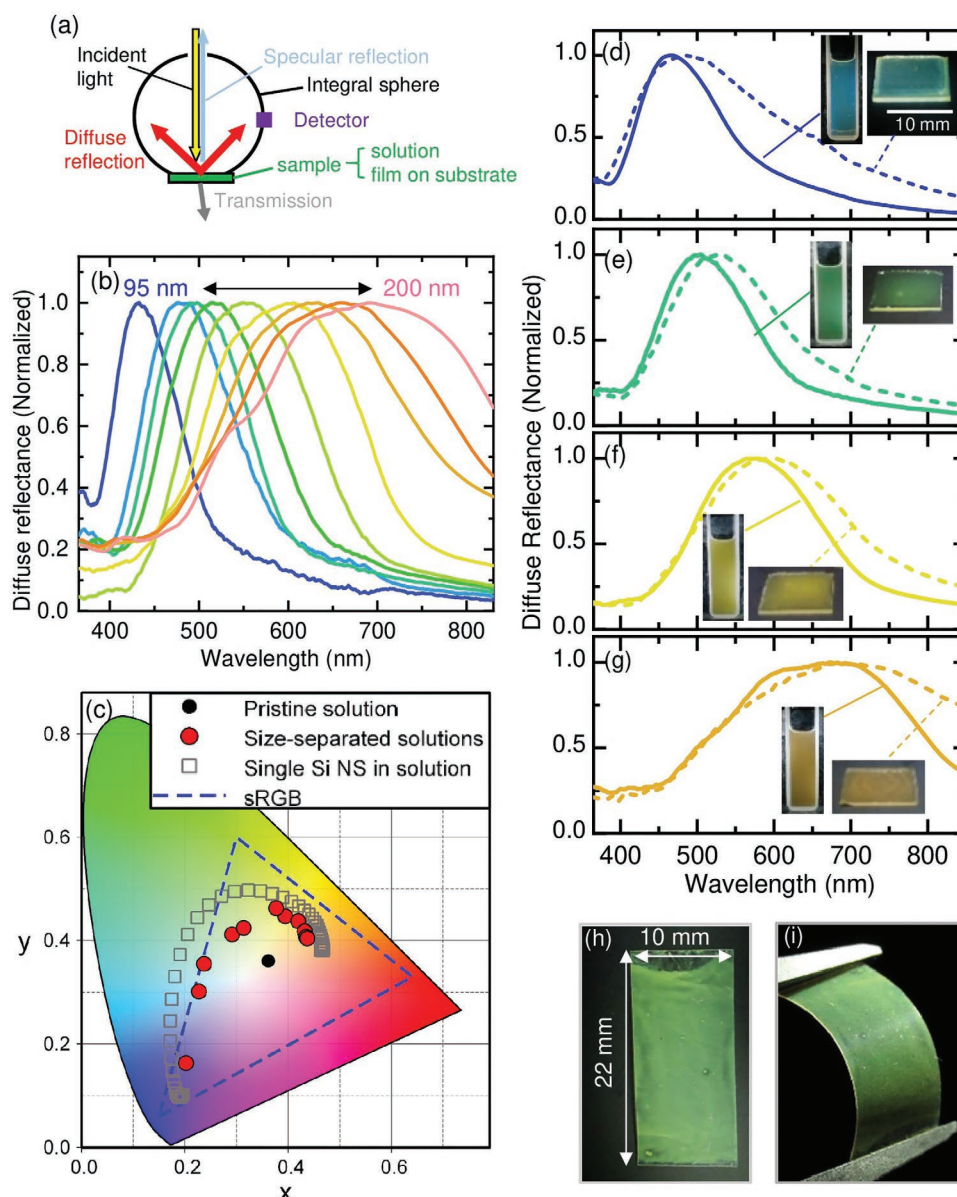


**Figure 4.** a) Experimental setup for diffuse reflectance measurements. b) Normalized diffuse reflectance spectra of solutions of size-separated Si NSs. c) CIE1931 chromaticity diagram and color space values obtained from diffuse reflectance spectra in (a) (red filled circles). Black filled circle corresponds to pristine solution. Data obtained from calculated spectra of single Si NSs in solutions are also shown (gray open squares). Diameters are changed from 95 to 200 nm. d–g) Photographs and normalized diffuse reflectance spectra of solutions of size-separated Si NSs (solid curves) and Si NSs-PVP films deposited on glass substrates (dashed curves). h) Photograph of Si NSs-PVP film on PET substrate. i) Photograph of Si NSs-PVP film on PET substrate bent at bending radius of 9 mm.

successful production of the color inks. The first one is the employment of SiO powder as the starting material, which solves the problem of scalability for mass production. The second one is the disproportionation of SiO at temperatures higher than the melting point of bulk Si crystal, which results in the growth of highly spherical Si particles with a circularity factor of 0.97 and perfect dispersion in solution without any agglomeration. The third one is precise size separation by the density gradient centrifugation process. Polydispersity as small as 6% is achieved. Thanks to the high sphericity, high crystallinity, high size purity, and perfect dispersion in a solution, the

Si NS solutions exhibit vivid color recognizable by the naked eye in a range of blue to orange. The Si NS color inks combined with a polymer binder are capable of coloring flexible substrates by a painting process.

#### 4. Experimental Section

*Preparation of Colloidal Dispersion of Si Nanoparticles:* Si NPs were prepared by thermal disproportionation of SiO. SiO lumps (several mm in size) (Wako, 99.9%) were crushed to powder and annealed at different

temperatures (1350–1600 °C) in a N<sub>2</sub> gas atmosphere for 10–30 min to grow crystalline Si NPs in SiO<sub>2</sub> matrices. Si NPs were liberated from SiO<sub>2</sub> matrices by etching in HF solution (46 wt%) for 1 h. Liberated NPs were then transferred to methanol and subsequently subjected to a minute sonication with an ultrasonic homogenizer (Violamo SONICSTAR 85). All processes were performed in an ordinary laboratory environment.

**Structural Characterization of Si Nanospheres:** Samples for TEM observations were prepared by dropping solutions of Si NSs onto carbon-coated copper grids. TEM, HAADF-STEM, and STEM-EDS mapping images were obtained using a JEM-2100F STEM (JEOL) operating at 200 kV. For the Raman scattering measurements, a solution of Si NSs was dropped on a gold-coated Si wafer, and a micro-Raman setup was used for the measurements (50× objective lens, NA = 0.8). The excitation source was 514.5-nm line of Ar<sup>+</sup> laser. To avoid sample heating, the laser power at the sample point was reduced to 0.1 mW by using an optical filter.

**Optical Characterization of Single Si Nanospheres:** A custom-built inverted optical microscope was used for dark-field scattering measurements of single Si NSs. Si NSs placed on a fused silica substrate were placed facedown onto the stage and illuminated by a halogen lamp via a dark-field objective lens (50×, NA = 0.8). The scattered light was collected by the same objective lens. Scattering images of Si NSs were obtained by a color CCD camera under illumination corrected by a neutral color balance filter. To measure the spectra, the scattered light was transferred to the entrance slit of a monochromator (SpectraPro-300i, Acton Research Corp.) and detected by a liquid-N<sub>2</sub>-cooled CCD (Princeton Instruments). The spectral response of the system was corrected by the scattering spectrum of a diffuse reflectance standard (Spectralon PP-100-SL).

**Calculation of Scattering Spectra of Si Nanospheres:** Scattering cross-sections of Si NSs with different diameters placed in air with a refractive index of 1 were calculated using the analytical equation of the Mie theory. The complex permittivity of Si crystal<sup>[36]</sup> was used. To reproduce the experimental scattering spectra, an experimental incident angle and a detection cone (NA = 0.8) were considered.

**Size Separation of Colloidal Si Nanospheres and Coloring Substrates:** Sucrose density gradient solutions were prepared by carefully adding 600-μL sucrose solutions at three different concentrations (45, 42.5, and 40 wt%) to a 2-mL centrifugal tube in order. The colloidal dispersion of Si NSs (150 μL) was added to the top of the tube, and the tube was the subject of centrifugation at 4500 rpm for 25 min to form layers of size-separated Si NSs. The layers were retrieved from the top and transferred to different vials. The solutions of size-separated Si NSs were washed with methanol several times to remove sucrose.

To color a substrate using Si NS inks, 10 μL of a methanol solution of PVP (10 wt%) was added to 100 μL of Si NS solution (≈0.01 mg mL<sup>-1</sup>) as the binder. The mixture solution was drop-cast onto silica or PET substrates and dried in air. The diffuse reflectance spectra of the inks in glass cuvettes (optical path of 2 mm) and coated films on glass substrates were measured by a spectrophotometer equipped with an integrating sphere (SolidSpec 3700, Shimadzu).

## Supporting Information

Supporting Information is available from the Wiley Online Library or from the author.

## Acknowledgements

The authors acknowledge Tatsuki Hinamoto for assisting with Mie calculations of Si nanospheres. H.S. acknowledges the support provided by JST, PRESTO Grant Number JPMJPR19T4, Japan. M.F. acknowledges the support of JSPS KAKENHI Grant Numbers 16H03828 and 18KK0141. This work was also partly supported by the Hosokawa Powder Technology Foundation.

## Conflict of Interest

The authors declare no conflict of interest.

## Keywords

colloid, Mie resonance, nanoparticles, silicon, structural color

Received: January 6, 2020

Revised: March 1, 2020

Published online: April 20, 2020

- [1] P. Vukusic, J. R. Sambles, *Nature* **2003**, 424, 852.
- [2] S. Kinoshita, S. Yoshioka, *ChemPhysChem* **2005**, 6, 1442.
- [3] H. Kim, J. Ge, J. Kim, S. Choi, H. Lee, H. Lee, W. Park, Y. Yin, S. Kwon, *Nat. Photonics* **2009**, 3, 534.
- [4] Y. Zhao, Z. Xie, H. Gu, C. Zhu, Z. Gu, *Chem. Soc. Rev.* **2012**, 41, 3297.
- [5] A. Kristensen, J. K. W. Yang, S. I. Bozhevolnyi, S. Link, P. Nordlander, N. J. Halas, N. A. Mortensen, *Nat. Rev. Mater.* **2017**, 2, 16088.
- [6] X. Zhu, C. Vannahme, E. Højlund-Nielsen, N. A. Mortensen, A. Kristensen, *Nat. Nanotechnol.* **2016**, 11, 325.
- [7] K. Kumar, H. Duan, R. S. Hegde, S. C. W. Koh, J. N. Wei, J. K. W. Yang, *Nat. Nanotechnol.* **2012**, 7, 557.
- [8] M. Miyata, H. Hatada, J. Takahara, *Nano Lett.* **2016**, 16, 3166.
- [9] S. J. Tan, L. Zhang, D. Zhu, X. M. Goh, Y. M. Wang, K. Kumar, C.-W. Qiu, J. K. W. Yang, *Nano Lett.* **2014**, 14, 4023.
- [10] J. Olson, A. Manjavacas, L. Liu, W.-S. Chang, B. Foerster, N. S. King, M. W. Knight, P. Nordlander, N. J. Halas, S. Link, *Proc. Natl. Acad. Sci. USA* **2014**, 111, 14348.
- [11] A. I. Kuznetsov, A. E. Miroschnichenko, Y. H. Fu, J. Zhang, B. Luk'yanchuk, *Sci. Rep.* **2012**, 2, 492.
- [12] V. Flauraud, M. Reyes, R. Paniagua-Domínguez, A. I. Kuznetsov, J. Brugger, *ACS Photonics* **2017**, 4, 1913.
- [13] C. S. Park, V. R. Shrestha, W. Yue, S. Gao, S. S. Lee, E. S. Kim, D. Y. Choi, *Sci. Rep.* **2017**, 7, 2556.
- [14] Y. Nagasaki, M. Suzuki, J. Takahara, *Nano Lett.* **2017**, 17, 7500.
- [15] Z. Dong, J. Ho, Y. F. Yu, Y. H. Fu, R. Paniagua-Domínguez, S. Wang, A. I. Kuznetsov, J. K. W. Yang, *Nano Lett.* **2017**, 17, 7620.
- [16] S. Sun, Z. Zhou, C. Zhang, Y. Gao, Z. Duan, S. Xiao, Q. Song, *ACS Nano* **2017**, 11, 4445.
- [17] D. G. Baranov, D. A. Zuev, S. I. Lepeshov, O. V. Kotov, A. E. Krasnok, A. B. Evlyukhin, B. N. Chichkov, *Optica* **2017**, 4, 814.
- [18] Y. H. Fu, A. I. Kuznetsov, A. E. Miroschnichenko, Y. F. Yu, B. Luk'yanchuk, *Nat. Commun.* **2013**, 4, 1527.
- [19] A. B. Evlyukhin, S. M. Novikov, U. Zywietz, R. L. Eriksen, C. Reinhardt, S. I. Bozhevolnyi, B. N. Chichkov, *Nano Lett.* **2012**, 12, 3749.
- [20] M. Caldarola, P. Albella, E. Cortés, M. Rahmani, T. Roschuk, G. Grinblat, R. F. Oulton, A. V. Bragas, S. A. Maier, *Nat. Commun.* **2015**, 6, 7915.
- [21] J. van de Groep, T. Coenen, S. A. Mann, A. Polman, *Optica* **2016**, 3, 93.
- [22] R. Regmi, J. Berthelot, P. M. Winkler, M. Mivelle, J. Proust, F. Bedu, I. Ozerov, T. Begou, J. Lumeau, H. Rigneault, M. F. García-Parajó, S. Bidault, J. Wenger, N. Bonod, *Nano Lett.* **2016**, 16, 5143.
- [23] G. H. Lee, S. H. Han, J. Bin Kim, J. H. Kim, J. M. Lee, S.-H. Kim, *Chem. Mater.* **2019**, 31, 8154.
- [24] S. Kim, V. Hwang, S. G. Lee, J. Ha, V. N. Manoharan, G. Yi, *Small* **2019**, 15, 1900931.
- [25] C. Zaza, I. L. Violi, J. Gargiulo, G. Chiarelli, L. Schumacher, J. Jakobi, J. Olmos-Trigo, E. Cortes, M. König, S. Barcikowski, S. Schlücker,



- J. J. Sáenz, S. A. Maier, F. D. Stefani, *ACS Photonics* **2019**, *6*, 815.
- [26] L. Shi, T. U. Tuzer, R. Fenollosa, F. Meseguer, *Adv. Mater.* **2012**, *24*, 5934.
- [27] L. Shi, J. T. Harris, R. Fenollosa, I. Rodriguez, X. Lu, *Nat. Commun.* **2013**, *4*, 1904.
- [28] W. Chaâbani, J. Proust, A. Movsesyan, J. Béal, A.-L. Baudrion, P.-M. Adam, A. Chehaidar, J. Plain, *ACS Nano* **2019**, *13*, 4199.
- [29] H. Sugimoto, M. Fujii, *Adv. Opt. Mater.* **2017**, *5*, 1700332.
- [30] H. Sugimoto, T. Hinamoto, M. Fujii, *Adv. Opt. Mater.* **2019**, *7*, 1900591.
- [31] Y.-J. Lee, N. B. Schade, L. Sun, J. A. Fan, D. R. Bae, M. M. Mariscal, G. Lee, F. Capasso, S. Sacanna, V. N. Manoharan, G.-R. Yi, *ACS Nano* **2013**, *7*, 11064.
- [32] Z. Iqbal, S. Veprek, *J. Phys. C: Solid State Phys.* **1982**, *15*, 377.
- [33] T. Matsukata, N. Matthaikakakis, T. Yano, M. Hada, T. Tanaka, N. Yamamoto, T. Sannomiya, *ACS Photonics* **2019**, *6*, 2320.
- [34] S. H. Lee, B. K. Salunke, B. S. Kim, *Biotechnol. Bioprocess Eng.* **2014**, *19*, 169.
- [35] J. Proust, F. Bedu, B. Gallas, I. Ozerov, N. Bonod, *ACS Nano* **2016**, *10*, 7761.
- [36] D. E. Aspnes, A. A. Studna, E. Kinsbron, *Phys. Rev. B* **1984**, *29*, 768.